Journal of the Korean Astronomical Society
50: 139 ∼ 149, 2017 October

https://doi.org/10.5303/JKAS.2017.50.5.139
pISSN: 1225-4614 · eISSN: 2288-890X
http://jkas.kas.org

Toward a Next Generation Solar Coronagraph: Development of a Compact Diagnostic Coronagraph for the ISS

K.-S. Cho[1,2], S.-C. Bong[1], S. Choi[1], H. Yang[1], J. Kim[1], J.-H. Baek[1], J. Park[1], E.-K. Lim[1], R.-S. Kim[1], S. Kim[1], Y.-H. Kim[1], Y.-D. Park[1], S.W. Clarke[3], J.M. Davila[4], N. Gopalswamy[4], V.M. Nakariakov[5], B. Li[6], and R.F. Pinto[7]

[1]Korea Astronomy and Space Science Institute, 776 Daedukdae-ro, Yuseong-gu, Daejeon 34055, Korea; kscho@kasi.re.kr
[2]University of Science and Technology, 217 Gajeong-ro, Yuseong-gu, Daejeon 34113, Korea
[3]NASA Headquarters, Washington DC 20546-0001, USA
[4]NASA Goddard Space Flight Center, Greenbelt, Maryland, USA
[5]University of Warwick, Coventry CV4 7AL, UK
[6]Sandong University, 27 Shanda Nanlu, Jinan, Shandong 250100, China
[7]Université de Toulouse, UPS-OMP, IRAP, 31400 Toulouse, France

Received July 2, 2017; accepted August 7, 2017

Abstract: The Korea Astronomy and Space Science Institute plans to develop a coronagraph in collaboration with National Aeronautics and Space Administration (NASA) and to install it on the International Space Station (ISS). The coronagraph is an externally occulted one-stage coronagraph with a field of view from 3 to 15 solar radii. The observation wavelength is approximately 400 nm, where strong Fraunhofer absorption lines from the photosphere experience thermal broadening and Doppler shift through scattering by coronal electrons. Photometric filter observations around this band enable the estimation of 2D electron temperature and electron velocity distribution in the corona. Together with a high time cadence (<12 min) of corona images used to determine the geometric and kinematic parameters of coronal mass ejections, the coronagraph will yield the spatial distribution of electron density by measuring the polarized brightness. For the purpose of technical demonstration, we intend to observe the total solar eclipse in August 2017 with the filter system and to perform a stratospheric balloon experiment in 2019 with the engineering model of the coronagraph. The coronagraph is planned to be installed on the ISS in 2021 for addressing a number of questions (e.g., coronal heating and solar wind acceleration) that are both fundamental and practically important in the physics of the solar corona and of the heliosphere.

Key words: instrumentation: coronagraph — Sun: corona — solar wind — acceleration of particles — space vehicles: International Space Station

1. Introduction

A coronal mass ejection (CME) is an abrupt, tremendous explosion of hot coronal plasmas, and can even be a threat to near-Earth environments especially when it interacts with Earth's magnetosphere. One of the severe effects of solar CME is the occurrence of geomagnetic storms, which can cause a variety of negative effects such as the disruption of electrical systems and communications, satellite hardware damage, malfunction of navigation systems, and radiation hazards affecting humans. In order to be prepared for such severe disruptions caused by CMEs, constant monitoring of solar activity and space environment conditions is crucial, and a coronagraph is the most essential instrument for such purposes. However, the Large Angle and Spectrometric Coronagraph (LASCO) aboard the Solar and Heliospheric Observatory satellite (SOHO), the only coronagraph currently in operation for CME observations in the Sun–Earth path, is more than 20 years old and is facing a discontinuance of operation in the near future.

Corresponding author: K.-S. Cho

So far this white light coronagraph has contributed to the increase of our knowledge about CMEs such as structures (e.g., Illing & Hundhausen 1985), angular widths (e.g., Howard et al. 1985), and velocities (Yashiro et al. 2004). In the middle of a general consensus in the international solar physics community about the requirement of a new space-based coronagraph, National Aeronautics and Space Administration (NASA) suggested the cooperative development of a next generation compact coronagraph for the International Space Station (ISS) to the Korea Astronomy and Space Science Institute (KASI) in 2013. While current coronagraph images provide electron density, the new coronagraph will utilize spectral information to also determine the electron temperature and flow velocity. Motivated by this suggestion, KASI conducted a planning study on a compact coronagraph for ISS in 2013 and subsequently a precedent study on the coronagraph in 2014. Furthermore, KASI and NASA organized a working group between the Solar and Space Weather Group in KASI and Heliophysics Division in NASA for an efficient and active collaboration. KASI started a new five-year space project to develop the coronagraph for the

ISS from 2017 in collaboration with NASA. Through this space project, KASI expects to contribute to the excellent scientific achievements of the solar community in the research fields of solar corona and CMEs. This coronagraph would be suitable for tracking wind speeds continuously in the acceleration region. Furthermore, the outcome of this project will contribute significantly to space weather forecasting for the long-term aim of public safety and protection of our space assets.

The Next Generation Coronagraph (NGC) developed through this project is expected to expand the current capability of coronagraph such as SOHO/LASCO. The new coronagraph derives new physical parameters that cannot be obtained using the current instrument. This will enable studies on solar wind dynamics including wave processes and turbulence, CME kinematics, and significantly improve the heliospheric corona-solar wind-CME model.

The rest of the paper is organized as follows. In Section 2, we briefly describe the scientific context and motivation. The mission overview of our project is presented in Section 3, and the instrument and evaluation plan are given in Section 4. A brief summary and outlook are delivered in Section 5.

2. SCIENCE CONTEXT AND MOTIVATION

The region of the corona in the field of view (FOV; 3 – 15 $R_\odot$) of NGC is of interest for addressing a number of important questions, both fundamental and practically important not only in solar corona physics but also in space weather forecasting. Given its capabilities, the coronagraph is expected to yield novel crucial insights into some long-standing puzzles in the physics of the solar wind. A non-exclusive list of such questions expected to be addressed by the coronagraph is as follows.

Q1. The acceleration of the fast and slow winds; radial profile of the bulk outflow velocities and their evolution; precise heights of the sonic and Alfvénic points for different heliospheric latitudes; link between different flow regions and the underlying low-coronal plasma structures (coronal holes, plumes, active regions, closed corona, etc.).

Q2. The heating of the plasma electrons; radial profiles of the electron, proton, and ionic temperatures.

Q3. The onset and development of plasma turbulence; partition of incompressive and compressive turbulence and their spectra, and evolution of these properties with the radial distance; details of the nonlinear cascade.

Q4. The appearance of coherent structures; e.g., macroscopic vortices.

Q5. The evolution of CMEs; nature of the aerodynamic drag force and its link with the turbulence.

Q6. The evolution of magnetohydrodynamic (MHD) waves; relationship between the MHD waves observed in-situ in the solar wind and the waves detected in the lower corona; energy flux, its dissipation and role in heating; wave-wave interaction; negative energy phenomena.

Some of these questions are linked to others; for example, Q6 is linked to Q1 and Q2: the waves are considered as one of the mechanisms for fast wind acceleration and plasma heating, whereas the specific profiles of the macroscopic (and, possibly, microscopic; e.g., particle beams) plasma parameters and their structuring directly affect the MHD wave dynamics.

2.1. Origin of Solar Winds and their Acceleration

There have been two long-standing inter-related issues in solar wind physics. The first issue regarding the origin of solar wind on the Sun; in other words, regarding the source regions of the solar wind. The studies on this aspect have a long history since as early as the 1970s (Fu et al. 2015). Fast wind is largely associated with coronal holes and slow wind may originate either in the open field regions adjacent to the coronal streamers or in the closed field regions (Abbo et al. 2016). However, no definitive answer is known regarding the precise properties of contribution of each potential source to the solar wind. Further, there are no routine measurements of the velocity field in the heliospheric range between 3 and 8 $R_\odot$. Above coronal holes, the Ultraviolet Coronagraph Spectrometer (UVCS) measurements do not extend beyond 3.5 $R_\odot$, for example. While, in principle, UVCS can measure the velocity profile along the streamer stalks up to 10 $R_\odot$, such measurements are very rare. Using the electron velocity field and the measurement of electron densities in the planned FOV, it will be possible to quantify the contribution of each potential wind source to the mass supply of the solar wind.

The second issue is to determine how the nascent solar wind is accelerated to several hundred kilometers per second within 10 $R_\odot$, for example. It is generally believed that, when leaving the Sun, the fast wind velocity is of the order of several kilometers per second (Hassler et al. 1999). The fast wind is already fully accelerated within 10 $R_\odot$, achieving a velocity of 700 $\mathrm{km\,s^{-1}}$ (Grail et al. 1996). A crucial clue to solving the acceleration of the fast wind is obtained from the measurements of the ion temperatures above the coronal holes, which were largely obtained by UVCS. As summarized by Cranmer (2002, 2009), ions are hotter than electrons, and their perpendicular temperatures tend to be higher than their parallel temperatures. This indicates that the rapid acceleration of the nascent fast wind may be a result of the proton pressure gradient force, which in turn results from the heating mechanisms that prefer protons over electrons. Notably, this scenario is in stark contrast to the original idea in Parker (1958), where the Parker wind is essentially driven by electrons (or, more precisely, via electron heat conduction). Regarding the slow winds, it appears that their acceleration in the near-Sun region is more gradual and is not complete until 20 $R_\odot$ (Wang et al. 2000). However, given the difficulties in observationally identifying the source regions of the slow winds, there is substantial controversy regarding the mechanisms responsible for their acceleration. If they arise from the open field regions just

outside the coronal streamers, then the UVCS measurements indicate a result similar to the fast wind above the coronal holes, i.e., ions are hotter than electrons, and ion perpendicular temperatures are higher than their parallel temperatures. This indicates that the acceleration of the nascent fast and slow winds could share a common acceleration mechanism. The substantial difference in their in situ properties may be either owing to the different lateral expansion rates (Cranmer et al. 2007) or different curvature radii (e.g., Li et al. 2011) of the coronal magnetic field lines along which the winds flow. On the other hand, the velocity profiles of the slow winds (Wang et al. 2000) can also be reproduced with the simple Parker model. This indicates that it remains to be seen whether the slow winds are driven by protons or electrons.

2.2. Coronal Heating

Electron temperature measurements in the FOV of NGC are extremely rare. The measurements from NGC, when compared with the UVCS measurements of ion temperatures closer to the Sun, will facilitate the assessment of whether the slow winds are distinct from the fast winds. Moreover, the power spectra of electron density fluctuations will be important in understanding compressible turbulence. Such spectra have never been obtained using remote-sensing data. Moreover, measuring the electron densities can shed new light on the compressible turbulence. So far, the analysis of solar wind turbulence primarily uses the magnetic field measurements made in situ, and they mostly concern incompressible turbulence. If it is possible to clearly identify an inertial range in the power spectra of electron density fluctuations as measured by the coronagraph, it is possible to evaluate the energy transfer rate. This will facilitate the evaluation of the importance of compressible turbulence in heating the solar wind. There is no need to fully resolve the inertial range; a partial resolving will suffice for this purpose.

Theoretically, Alfvén waves were intensively studied in the context of coronal heating (Alfvén 1947). Despite several claims of the observational detection of Alfvén waves in the solar corona in the literature, these waves have not been unequivocally detected yet. They have been often confused with kink waves, which are of fast magnetoacoustic nature. Further, Alfvén waves should be abundant in the corona, since they can be readily generated by photospheric motions and then propagated upward without reflection, refraction, or strong dissipation. The difficulties with their detection are mainly connected with their non-collective nature: Alfvén oscillations of neighboring magnetic surfaces are completely disconnected with each other. Moreover, even if Alfvén waves are excited in phase on a large number of magnetic surfaces, they rapidly become out of phase with each other owing to the difference in the local Alfvén speeds – the effect of Alfvén wave phase mixing. The spectrum of the outward propagating Alfvén waves is not known, and it may evolve owing to mode coupling and nonlinear cascade. Alfvén waves can be considered as the non-thermal broadening of the absorption lines observed in the Thomson scattering with NGC, by unresolved motions. In the low corona, the amplitude of transverse flows estimated by the non-thermal broadening reaches approximately 130 km s^{-1} at the height of 10 $R_\odot$ (e.g., see Figure 9 in Cranmer & van Ballegooijen 2005). Linearly or elliptically polarized Alfvén waves induce bulk flows of the plasma outwards from the Sun by the ponderomotive force and the effect is referred to as the "Alfvénic wind". The relative amplitude of the induced field-aligned outward flows, e.g., the ratio of the density fluctuations to the background density, is proportional to the square of the relative amplitude of the mother Alfvén waves, and inversely proportional to the difference of the local Alfvén and sound speeds (e.g., Nakariakov et al. 2000). Thus, the relative amplitude of the induced compressive perturbations increases in the vicinity of the height where the sound speed becomes almost the same as the Alfvén speed. If the mother Alfvén waves are harmonic, the period of the variations of the induced field-aligned flow is half of the Alfvén wave period. These induced density variations can be observed using the NGC. Therefore, the search for coronal Alfvén waves in non-thermal broadening and caused by the induced compressive fluctuations is an interesting task for the NGC.

2.3. MHD Seismology

MHD seismology is a rapidly developing diagnostic technique of various plasma structures, which probes the plasma parameters. It provides us with information about the processes operating there, by means of MHD waves. The very nature of MHD seismology is the synthesis of observations using advanced theoretical modeling of the interaction of MHD waves with the plasma. The success of MHD seismology is based on the use of observational facilities with high precision and sensitivity.

The radial speed of the CME progression is observed to vary quasi-periodically. Michalek et al. (2016) performed a statistical study of this phenomenon in 187 limb CMEs observed with LASCO, and concluded that 22% of the CMEs observed in the years 1996 – 2004, revealed periodic velocity fluctuations with an average amplitude of 87 km s^{-1}, mean period of 241 min, and wavelength of 7.8 $R_\odot$. Lee et al. (2015) observed similar kinematic oscillations in halo CMEs observed using LASCO, and found quasi-periodic variations of the instantaneous radial velocity with periods ranging from 24 to 48 min. The oscillations correspond to different azimuthal modes, mainly $m = 0$ and $m = 1$. The oscillation period is found to be inversely proportional to the amplitude and the projected speed of the CME. The nature of these kinematic oscillations has not been understood yet. The possible options are MHD oscillations (in case the plasmoid is still magnetically linked to the Sun), and the periodic shedding of Alfvén vortices (see Lee et al. 2015 for a discussion). One may also expect some periodic variation of the aerodynamic drag force; however, there is no theoretical modeling of this

phenomenon. The relationship between the oscillation period and amplitude indicates the nonlinear nature of this phenomenon. Kinematic oscillations of CMEs have a broad range of periods, i.e., 0.5 – 7 h, and they are well resolved using LASCO/C2 and C3. Hence, they should be detectable with the coronagraph. It would be relevant to scientific questions Q1, Q3, Q4, and Q5.

Quasi-periodic rapidly propagating wave trains of the EUV intensity variations were recently discovered using the Atmospheric Imaging Assembly (AIA) on the Solar Dynamics Observatory (SDO) (Liu et al. 2011). The typical periods were 1 – 2 min, and the typical speeds were 1000 – 2000 km s^{-1}. Pascoe et al. (2013) demonstrated that these waves appear naturally after a broadband excitation of fast magnetoacoustic waves in a field-aligned plasma waveguide. The waveguide can be a plasma non-uniformity such as a magnetic funnel, polar plume, streamer, pseudo-streamer, or another structure of this kind. The waves are guided outwards from the Sun by the waveguide, and hence do not come back, since they do not experience the refraction caused by the vertical non-uniformity of the corona. The oscillation period is determined by the fast magnetoacoustic transit time across the non-uniformity at the point of the excitation. Goddard et al. (2016) compared the EUV and radio observations, and found out that the fast magnetoacoustic wave trains reach the height of at least 0.7 $R_\odot$. Ofman et al. (1997) detected 9.5 min oscillations of the white-light pB in polar coronal holes at the height of 1.9 $R_\odot$ using the SOHO/UVCS. In the spectrum, there are also possible peaks at longer periods (40 – 60 min). Moreover, similar quasi-periodic features could develop and be detected in streamers and pseudo-streamers after the impact of a CME. For example, Kwon et al. (2013) observed swing motions of a streamer for 90 – 130 min at heliocentric distances of 1.6 – 3 $R_\odot$ using STEREO/SECCHI/COR1. The speed of the outward-propagating kink-like displacement of the streamer increased from 500 to 1600 km s^{-1}. It is possible that the fast wave trains could reach the NGC FOV. Thus, the study of quasi-periodic rapidly propagating compressive wave trains using NGC appears to be a realistic task. It would be relevant to science questions Q1 and Q6.

2.4. Thermodynamics of CME and Other Coronal Structures

The proposed coronagraph filter system is very different compared with existing coronagraph instruments. We have mainly used white light coronagraph images to determine the geometric and kinematic parameters of coronal structures. Our goal is to determine other parameters of the coronal structures using the coronagraph filter system. Among these new parameters, we expect temperature to be the most useful quantity. Previous studies proposed a few methods to measure the coronal temperature. The most representative method is spectroscopic observation using the Coronal Diagnostic Spectrometer (CDS) or the UVCS on board the SOHO. However, many cases were not observed, and especially in the case of CMEs, this method is limited by the temporal and spatial randomness in the occurrence of CMEs. Therefore, a coronagraph that can observe a large FOV continuously is highly advantageous for the temperature measurement of CMEs or other coronal structures. As a case study, Cho et al. (2016) simulated the expected observation result. They restored a structure of the CME that occurred on January 4, 2002 by using the graduated cylindrical shell model (Thernisien et al. 2006). By considering the geometrical parameters of the CME and assuming the isothermal CME temperatures in the range between 0.5 and 2.0 MK, they calculated two filter intensity ratio images of the corresponding CME temperatures. Based on their simulation, they suggested that the filter intensity ratio is approximately in the range of 1.2 to 1.6, sufficiently large to be observed in a realistic measurement.

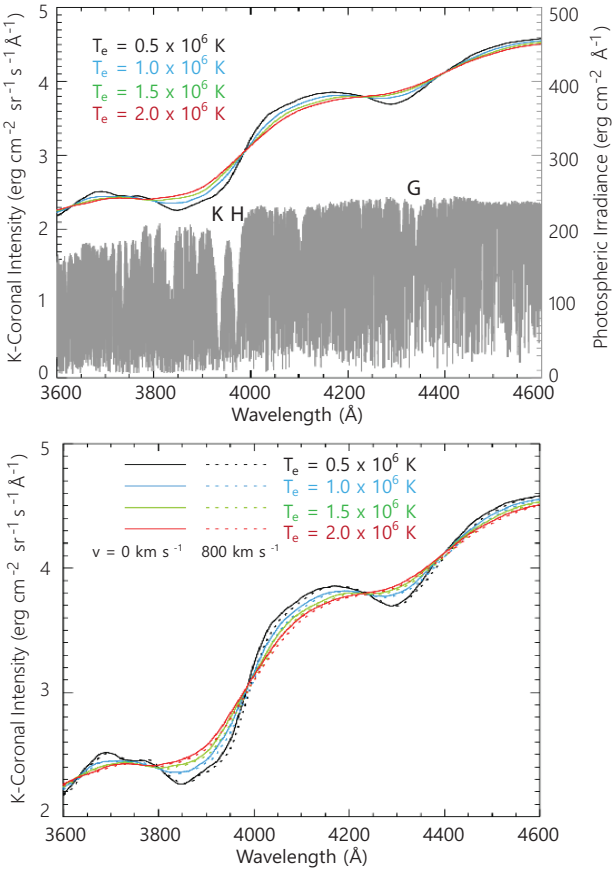

Figure 1. K-corona spectra at different temperatures and outflow velocities.

2.5. Solar Wind, CME Propagation, and Space Weather Forecast

The interplanetary medium is continuously swept by the solar wind and by different types of perturbations that propagate through it. Some of these perturbations are intrinsic to the quasi-steady background wind flow, or related to oscillatory motions introduced by continued surface movements and to impulsive phenomena occurring on the active corona. The global spatial (or

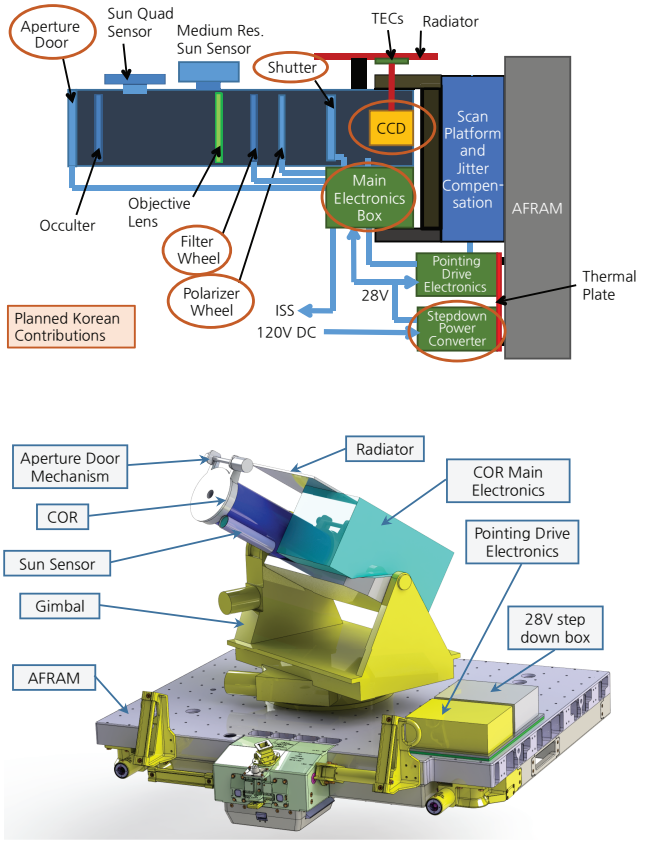

Figure 2. Block diagram (upper panel) and strawman design (lower panel) of the coronagraph on the ISS.

angular) distribution of fast and slow solar wind flows reflects to a great extent the geometry of the coronal magnetic field, which affects the heat, mass and momentum fluxes guided along the field (e.g., Wang & Sheeley 1990; Richardson & Kasper 2008). Solar rotation gives rise to interactions at the interfaces between neighboring fast and slow wind flows and to the formation of corotating density structures (CDS) at higher atmospheric altitudes (e.g., Plotnikov et al. 2016, and references therein). Planetary magnetospheres are bound to adapt continuously to the fluctuations of ram pressure associated with these flows, which cross them successively (even though this component of the solar wind is essentially quasi-stationary). CMEs and the associated shocks are a source of impulsive perturbations that add up to the softer but much more frequent background solar wind perturbations. The detailed physical properties of the background wind flow also play a major role on the propagation paths and delays of such CMEs and shocks, through friction and by setting the upstream phase speeds.

The sources of these physical processes lie in the dynamics of the lower layers of the solar atmosphere. The conditions for their development and outward propagation are mostly set at the solar corona, roughly between 2 and 10 $R_\odot$. Having access to velocity fields, plasma densities and temperatures at regular interval at all these altitudes is critical for space weather science. The understanding of the physics of the generation of earth-bound solar perturbations still faces major challenges and lacks observational constraints, in line with the scientific questions discussed in the previous subsections (and listed at the beginning of Section 2).

Over the years, the community has addressed the uncertainty relating to these processes by developing a combination of heuristic hypotheses, semi-empirical techniques (Wang & Sheeley 1990; Rotter et al. 2012; Fujiki et al. 2015) and global-scale 3D numerical models of the corona and solar wind (Lionello et al. 2001; Gressl et al. 2014; van der Holst et al. 2014; Yang et al. 2016; Pinto & Rouillard 2017). The vast majority of such models uses partial information about the state and/or evolution of the solar surface as a lower boundary condition. Typically surface magnetograms are extrapolated into the corona. Furthermore, those models need to rely on simplifying hypothesis for the top boundary conditions, as well as for the physical processes leading to the heating and acceleration of solar wind flows. Validation of the models relies critically on reproducing or forecasting solar wind speed time-series where they can be measured systematically, such as at the Sun-Earth Lagrangian point L1 (other orbital positions have also been used for the duration of specific missions, such as HELIOS, ULYSSES and STEREO). Radio surveying techniques (IPS; e.g., Tokumaru et al. 2010) give access to large-scale low resolution wind speed distribution in the heliosphere. However, comprehensive and high quality data sets relating directly to coronal heights – where the wind flows are heated and accelerated and where CMEs are triggered – are still rare (with the SOHO/UVCS coronograph being a remarkable exception; Kohl et al. 1998).

3. MISSION OVERVIEW

The ISS-COR will provide a series of plane-of-sky maps of the corona and solar wind between 3 and 15 $R_\odot$ with unprecedented quality and will therefore represent a major opportunity to test and improve the current knowledge about the physics of the corona and of the heliosphere. The planned launch in 2021 lets us foresee a great potential for synergy with other solar space missions in preparation (Solar Orbiter, Parker Solar Probe, PROBA-3) or in discussion (missions at the Lagrangian point L5).

3.1. Concept

While the current coronagraph provides electron density information through polarized white light images, the new coronagraph can also provide information about coronal temperature and velocity by observing multiple wavelengths. The basic concept is described as follows. Strong absorption lines of the visible light irradiated from the solar photosphere are flattened by the thermal motions of free coronal electrons. Thus, the electron temperature determines the amount of flatness of the absorption lines, which can be represented by the ratio of intensities in two temperature-sensitive wavelengths. Moreover, the radial motion of solar wind

Table 1
Performance specifications of the coronagraph

Parameter	Range
FOV ($R_\odot$)	15
Inner FOV cutoff ($R_\odot$)	3
Wavelength range (nm)	380 – 450
Effective focal length (mm)	103
Entrance pupil diameter (mm)	40
Detector array	CCD, 1950 × 1950, 7.4 μm pixel
Throughput (average over λ and FOV)	$> 90\%$
Mass	< 75 kg

affects the redshift of the entire coronal spectrum. The ratio of two velocity sensitive wavelength intensities also facilitates the estimation of the velocity of solar wind. The mathematical calculations are described in detail by Cram (1976) and Reginald (2001).

Figure 1 shows a result of the numerical code (Cho et al. 2016) that calculates the expected spectra from a given coronal temperature and velocity. Photospheric spectrum between 370 – 450 nm contains many absorption lines such as Fraunhofer G, H, and K lines as shown in the upper panel. These absorption lines experience thermal broadening and Doppler shift through scattering by coronal electrons. As shown in the lower panel, thermal broadening increases with the electron temperature and results in an increase in the intensity at the center of the absorption line and a decrease in the intensity near the absorption line. Therefore, we can estimate the coronal temperature by measuring intensity ratio between the center (e.g., 3850 Å) and the vicinity (e.g., 4100 Å) of a strong absorption line. The Doppler shift increases with the electron outflow velocity with respect to the photosphere, and results in an increase or decrease in the intensity at the wavelengths between the center and the vicinity of a strong absorption line, where the spectral slopes are steep (e.g., 3987 Å and 4233 Å). We can estimate the coronal outflow velocity by measuring the intensity ratio between the wavelengths of the steep spectral increase and decrease.

3.2. System Requirements

Figure 2 shows the block diagram and strawman design of the coronagraph, which consists of an optical assembly, filter and polarizer wheels, camera, and electronics box. The optical assembly consists of the lens group including a field lens, external occulter, and additional stray-light rejection arrangement. In the context of this overall project, NASA and KASI will design, build, and perform quality testing of the coronagraph and fly it on the ISS. NASA and KASI will employ reasonable efforts to carry out the following responsibilities.

NASA will: (a) manage and provide product assurance for the coronagraph development at Goddard Space Flight Center (GSFC); (b) coordinate procurement specifications, interface documents, and initiate procurement activities for long lead items required for the payload; (c) provide designs for the optical and mechanical assemblies of the coronagraph; (d) provide other engineering and technical services (e.g., thermal design, materials, configuration management, environmental test, quality) as needed; (e) participate in design reviews both in the USA and Korea; and (f) conduct environmental and performance testing.

KASI will: (a) design, build, and qualify the coronagraph door, filter wheel, filters, main electronics and camera electronics, including the interfaces with the ISS; (b) provide other engineering and technical services (e.g., thermal design, materials, configuration management, environmental test, quality) as needed for the KASI components; (c) participate in design reviews both in the US and Korea; and (d) support environmental and performance testing.

The observed field of view is up to 15 $R_\odot$ and the inner limit is 3 $R_\odot$, which is similar to that of STEREO/COR2. As the diagnostics of coronal electron temperature and velocity is expected to be applicable only up to 8 $R_\odot$, the inner limit is desired to be as low as that allowed by the the optical design and dynamic range. Table 1 summarizes the specifications of the coronagraph to achieve the main scientific purpose and observation target of this project. The image resolution is 14.8 arcsec. We will use a 2K × 2K CCD.

3.3. Work Scope and Roadmap

For collaboration with the coronagraph team at NASA, KASI will follow NASA procedures and guidance for the development of mechanisms, electronics box, and CCD detector. A control system compatible with the ISS standard interface will be developed by utilizing the core flight software (CFS) framework to combine hardware and software development. As shown in the KASI roadmap in Figure 3, our final goal is to develop a science-oriented coronagraph and install it on the ISS in 2021 for operation of more than 2 years. Prior to the installation on the ISS, we will perform experiments during a total solar eclipse (TSE) on the ground in 2017 to test the filter system and on a balloon in the stratosphere in 2019 to evaluate the engineering model for the ISS. The eclipse expedition is planned to test the filter system without using an occulter and will be conducted in August 2017 at Jackson in Wyoming, USA. The KASI–NASA working group agreed during the first working group meeting at NASA Headquarters in September 2016 that a balloon mission is the optimum path to increase the technological readiness level

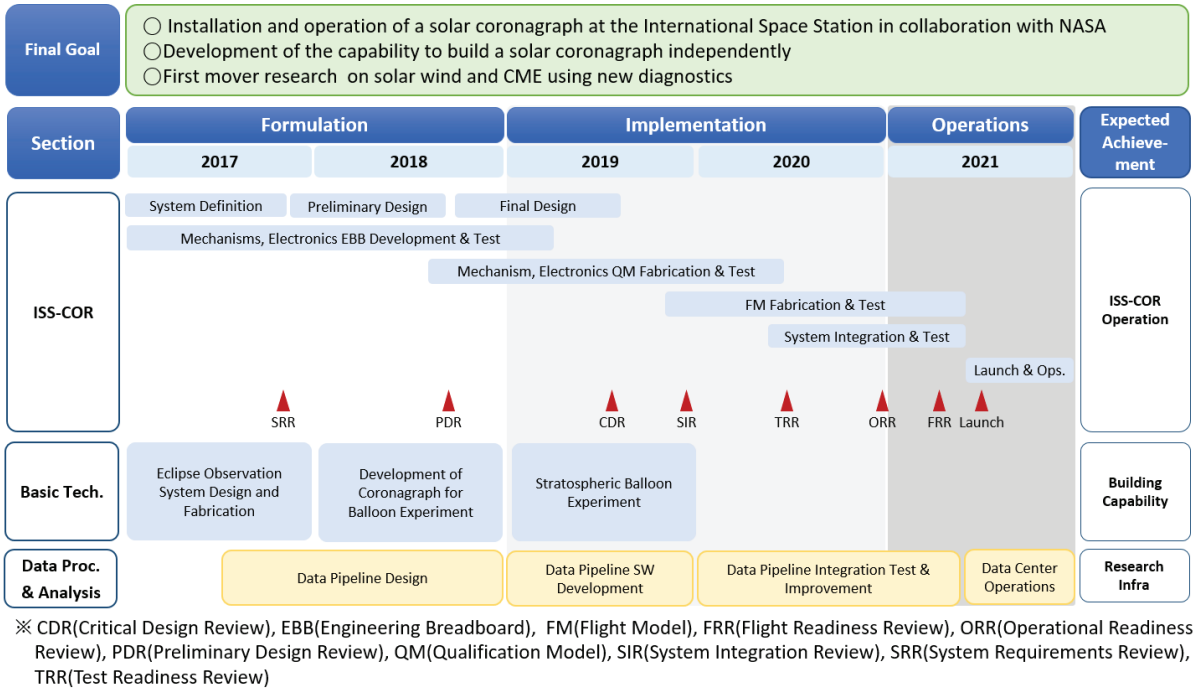

Figure 3. Timeline for the coronagraph development.

of the coronagraph for a future mission to be flown on the ISS. A stratospheric (< 40 km) balloon test in collaboration with NASA will be conducted using a pointing system, gondola, and balloon from NASA. In order to measure and reduce the diffraction light of the external occulter, we will conduct several experiments by using a small laboratory for the solar simulator and the normal pressure/vacuum solar simulator facilities of China and USA.

4. INSTRUMENT AND TESTING

4.1. Key Techniques

An occulting disk (OD) blocks the light from a solar disk to observe the much fainter solar corona. The classical externally occulted coronagraph consists of an external OD and an internal OD system. The diffraction light generated by the edge of the external OD exceeds the corona light so that it should be suppressed by the internal OD, which is located in the plane of the external OD image made by the objective lens. However, in this case, the overall length of the system should be up to few meters to archive several image planes. Recent studies have suggested that the diffraction light of the external OD can be reduced by changing its design. A saw-tooth-shaped and cone-shaped occulter have been investigated by several studies (Percell & Koomen 1962; Bout et al. 2000; Koutchmy 1988; Gong & Socker 2004). Such ODs can reduce the length of the system to shorter than 1 m, which is the key to the technology of the compact coronagraph or miniature coronagraph.

The corona brightness above 3 $R_\odot$ is approximately $10^{-10} I_\odot$ (November & Koutchmy 1996). Hence, the diffraction light of the occulter should be suppressed to below $10^{-10} I_\odot$. In the ISS coronagraph, we intend to use a cone-shaped external occulting disk (COD) without an internal occulting disk. A COD with a carefully chosen angle in its outer wall can significantly reduce the diffraction light caused by the light from the solar disk.

We have tested the performance of the occulter using the light source provided by the solar simulator and the laser, and subsequently with a simple source located 20 m away in open air. We observed that the singlet OD can suppress the diffraction light down to $10^{-6} I_\odot$. Subsequently, we performed the test for the cone-shaped occulter and confirmed that the diffraction light can be suppressed to approximately $10^{-7} I_\odot$ by using the COD. However, the stray light level of the experiment is slightly higher than $10^{-7} I_\odot$. The stray light was caused by the scattering at the baffle in the case of the solar simulator experiment, and the reflection of light at the wall and scattering by dust in the case of the far-away source experiment. It was essential to remove the stray light mathematically from the results. We will develop a COD optimized to reduce the stray light and repeat the experiment in the clean tunnel and the vacuum chamber with the real sun. After testing the COD in the ground experiment in the clean tunnel and the vacuum chamber, we will use the COD in the balloon coronagraph observation. The design of the COD can be adapted suitably for the balloon experiment.

The second key technology of the coronagraph is the filter system, which will provide the information of electron temperature and velocity in the solar corona. We have developed our own numerical code that calcu-

Table 2
Central wavelengths of filters

	Temperature measurement	Velocity measurement
Central wavelength	3900 Å, 4103 Å	3987 Å, 4233 Å

lates the expected spectra from a given coronal temperature and velocity. Furthermore, we determined the optimized wavelength of filters with a Gaussian response function for the coronal temperature and velocity measurements. We calculated the coronal spectra at 1.1 $R_\odot$ under the spherically symmetric coronal electron density model (Baumbach 1937) for various temperatures and radial velocities of coronal electrons. Subsequently, we obtained filter intensity ratios for various pairs of central wavelengths. For a temperature-sensitive filter, we chose a central wavelength pair that is sensitive to temperature variations and insensitive to velocity variations. The central wavelength pair for the velocity measurements was determined in a similar way. Table 2 summarizes our results.

Our calculation is based on a simple model and the optimum wavelengths may be different from our results. The specifications are different from the previous results in Reginald (2001) (3850 Å and 4100 Å for temperature, 3987 Å and 4233 Å for velocity). We find three potential reasons for this difference. First, we used solar spectral irradiance data from Kurucz (2005) as input, whereas Reginald (2001) used the data tabulated by the McMath/Pierce Solar Telescope facility at Kitt Peak, Arizona. Second, the integration method led to a difference. We replaced the trapezoidal rules in Reginald (2001) with Gaussian Legendre quadrature, which is more accurate and faster. Third, they calculated the intensity ratio at specific wavelengths, but we applied a Gaussian filter. The central wavelengths of the velocity measurement filters are similar to the result obtained by Reginald (2001), but slightly different for the temperature measurement. We will investigate a more realistic situation and determine the final wavelengths.

Although narrow filter are advantageous for a parameter measurement, we currently intend to use filters of 100 Å bandwidth to reduce the exposure time considering the weak coronal intensity. Moreover, solar wind velocity measurements through the coronagraph filter observation are expected to be challenging owing to the small variation of the filter intensity ratio. In order to overcome this difficulty, we intend to maximize the signal-to-noise ratio by optimizing the optical design and parts including the occulter, lens, filters, polarizers, and CCD sensors.

4.2. Experiments

The KASI–NASA working group of the ISS-COR agreed to perform TSE observation and a balloon experiment for the demonstration and validation of the coronagraph technology before the launch of the ISS-COR. Furthermore the working group shared NASA/GSFC and KASI TSE observation plans in 2017 and a view of the possible balloon flight in 2019 as a precursor mission or risk reduction flight to the ISS-COR launch. These risk-reduction plans summarized in Table 3 will be helpful to refine both the ISS-COR coronagraph instruments and the science objectives through testing of the technology and conducting early scientific experiments. Moreover, such a challenge would provide KASI with valuable experience regarding new instrumentation missions and the acquisition of balloon-borne pointing technology for future larger space missions.

4.2.1. TSE Observation

The date of the TSE in 2017 was August 21 across the USA. The greatest eclipse was at 18:25:32 UT in the west of Kentucky. The eclipse magnitude was 1.0306 and the greatest duration was 2 min 40 s in the south of Illinois. The greatest path width was 115 km. For the total eclipse observation, we did not use the external occulter, and there was no inner limit. The sky brightness during the totality was approximately $10^{-9} I_\odot$, overwhelming the corona brightness above 4 $R_\odot$. The sky was expected to be unpolarized (Hayes et al. 2001), and there was a possibility of observing polarization brightness (pB) up to 8 $R_\odot$. However, the innermost part of the corona was a thousand times brighter than the sky. We observed the eclipse at a site near Jackson, Wyoming, where the weather was good and the totality was not substantially shorter than its maximum duration. At the accommodation, the duration of totality was 2 min 17 s. Maximum eclipse occurred at 17:35:56 UT (11:35:56 MDT) and the altitude and the azimuth angles of the Sun were 50.4° and 135.6°, respectively. We used an optical system including the filter wheel, polarizer motion part, and CCD to test the key components of the NGC. Two camera mount assemblies for the filter wheel with the bandpass filters and the polarizer were mounted on a tripod to record the observations. We obtained several polarized brightness images in each filter and data analysis is ongoing to verify the fundamental technology of the NGC.

4.2.2. Balloon Experiment

The advantage of high-altitude, stratospheric balloon borne experiments is in their relatively low cost and quick launch compared to experiments using space satellites. Altitudes of higher than 30 km can provide scientific payloads with the good observing conditions of the corona, with reduced atmospheric scattering and attenuation effects. Therefore, a stratospheric balloon-borne experiment is a good preceding project to validate the scientific performance of the developed coronagraph

Table 3
Experiment and installation plan

	Total solar eclipse	Balloon flight	ISS installation
Year	2017	2019	2021
Altitude	Ground	Stratosphere (up to 40 km)	Low Earth Orbit (340 km)
Observing time	2 min 17 s	6 – 8 h	46 min per orbit
Environment temperature	—	−50 – 0 °C	−126 – 149 °C
Power	—	< 10 W	< 78 W
Mass	—	< 25 kg	< 75 kg

before the launch to ISS. The KASI and NASA coronagraph team will design, fabricate, test, and fly an engineering model of the coronagraph onboard a balloon to be launched by NASA's Columbia Scientific Balloon Facility (CSBF). The instrument consists of optical assembly, polarization camera, and electronics box. The optical assembly consists of a lens group including the field lens, the external occulter, and an additional stray-light rejection arrangement. NASA and KASI will design, build, and perform the qualification test of the coronagraph and fly it on a stratospheric balloon equipped with NASA's Wallops Arc Second Pointer (WASP). The tests of the coronagraph will be performed at GSFC and the National Center for Atmospheric Research (NCAR) vacuum chamber or the NASA Marshall Space Flight Center (MSFC) vacuum chamber. The coronagraph will be built, delivered to the Wallops Flight Facility (WFF) for integration into gondola and WASP system, and flown on the stratospheric balloon in September 2019 from Ft. Sumner, New Mexico.

4.2.3. ISS Experiment

Since November 2000, the ISS has been continuously operated by five participating space agencies: NASA, Russian Federal Space Agency, Japan Aerospace Exploration Agency, European Space Agency, and the Canadian Space Agency. The ISS maintains a low Earth orbit at an altitude between 330 km and 425 km with an inclination of 51.6° to the equator, completeing 15.51 orbits per day. In low Earth orbit, temperatures outside the ISS can vary from −126°C to 149°C. The integrated truss structure (ITS) of the ISS provides opportunities for external payloads. There are six sites available on the ITS, two of which have been allocated to the Alpha Magnetic Spectrometer (AMS) and the External Stowage Platform (ESP-3). The other four sites are assigned to ExPRESS Logistics Carriers (ELCs), which were developed by NASA as carriers that can be utilized to carry a variety of orbit replacement units, outfitting cargo, and external payloads for scientific experiments. We are considering the ELC-2, which is attached to the ITS S3 and available after mid-2019. The maximum mass allowed is approximately 227 kg for the payload itself and the orbit average power is approximately 750 W. The allowable physical volume for the external payload during on-board operation is 86.36 × 116.84 × 124.46 cm (length × width × height). Each external payload will be provided with two +120 Vdc heater power buses, a +120Vdc operational power bus, and an operational +28 Vdc power bus. At the interface between the ELC module and the payload interface, there are three data ports: high-rate-data link (HRDL), low-rate-data link (LRDL), and medium-rate data link (MRDL). Ethernet is used for the uplink MRDL, the transmission rate between the ELC module and the payload is up to 10 Mbps. The HRDL rate for downlink service to the ground is up to 95 Mbps. The LRDL is used for the data and command link between the ELC and the payload via the ELC avionics module at a maximum rate of 1 Mbps. Table 4 summarizes the ISS ELC-2 capability and the ISS-COR requirement. We will develop the coronagraph and a pointing system and install them on the ISS in 2021.

5. Summary and Outlook

KASI and NASA have been developing a solar coronagraph system, which is expected to be installed on the ISS. NASA has proposed a compact coronagraph which consists of an external occulter, compact lens group, four bandpass filters, and a polarizer camera. This design can facilitate the measurement of not only electron density, which can be obtained from current other coronagraph systems, but also the electron temperature and velocity of the solar wind. The key components of the coronagraph will be tested during the North-American total solar eclipse in 2017 and a qualification level model will be mounted on a stratospheric balloon to demonstrate and verify the space model requirements. The final coronagraph will be installed on the ISS to understand the structure and dynamics of the corona-heliosphere connection at all latitudes and eventually to constrain solar wind acceleration models. The observation of the radial temperature and velocity profile of solar wind from the top of closed streamers to the vicinity of the sonic point will provide answers to the questions listed in Section 2.

We employ bandpass filters that transmit wavelengths sensitive to temperature or velocity; consequently, we obtain light over a narrower wavelength band than current coronagraphs. Therefore, we may have difficulty in studying dynamic features such as very fast CMEs, owing to the extended exposure time to obtain sufficient photons. In order to overcome this problem, we intend to use two different observation modes: a diagnostics mode using narrow bandpass filters to determine temperature, velocity, and density,

Table 4
Comparison between ISS-COR requirement and ISS ELC-2 capability

Resource	ISS-COR Requirement (with 30 % contingency)	ISS ELC-2 Capability
Mass	75 kg	227 kg (200%)
Orbit Average Power	78 W	750 W (320%)
Orbit Average Data Rate	150 kbps (10 pB images, 2.5 compression)	6 Mbps (Ethernet) 1 Mbps (IEEE 1553) (560 %)
Volume	50 × 11 × 29 cm	86.36 × 116.84 × 124.46 cm

and a dynamics mode using a wide bandpass filter to observe the dynamic features of CMEs. The density is determined using pB, and the temperature is determined using image ratio between the temperature sensitive filter pairs. The velocity is determined in the same way by using velocity sensitive filter pairs. In the dynamics mode, we repeatedly observe the intensity through a wideband filter with higher cadence. We can study the dynamic features of a CME by subtracting the background intensity before or after the CME.

We are in favor of arranging joint observational campaigns with the observational facilities operating in other bands and/or observing other parts of the corona, exploiting complementarity. We expect that the coronagraph will provide observations of the radial profile of electron density, velocity, and temperature from 3 to 8 $R_\odot$ at all latitudes, which are critically important for the interpretation of the in-situ measurements by the Parker Solar Probe and Solar Orbitor and result in a significant improvement of the science return of the missions. In the radio band, interesting perspectives are offered by the simultaneous observations of CMEs, streamer blobs, and other moving coronal features using the ISS-COR and the LOw Frequency ARray (LOFAR). LOFAR is a European digital radio interferometer operating at 10–90 and 110–250 MHz with the time cadence of 1 s. Hence, for the radio waves created by the plasma emission, e.g., Type III bursts, it allows the imaging of the corona (including Faraday rotation and scintillation) in the region within 3 $R_\odot$ (e.g., Breitling et al. 2015), filling in the gap between the low corona observed in EUV and the ISS-COR observational heights ($3 \sim 15$ $R_\odot$).

ACKNOWLEDGMENTS

This work was supported by the Korea Astronomy and Space Science Institute under the R&D program (2017-1-851-00) supervised by the Ministry of Science, ICT, and Future Planning.

REFERENCES

Abbo, L., Ofman, L., Antiochos, S. K., Hansteen, V. H., Harra, L., Ko, Y.-K., Lapenta, G., Li, B., Riley, P., Strachan, L., von Steiger, R., & Wang, Y.-M. 2016, Slow Solar Wind: Observations and Modeling, Space Sci. Rev., 201, 55

Alfvén, H. 1947, Granulation, Magneto-Hydrodynamic Waves, and the Heating of the Solar Corona, MNRAS, 107, 211

Baumbach, S. 1937, Strahlung, Ergiebigkeit und Elektronendichte der Sonnenkorona, AN, 263, 120

Bout, M., Lamy, P., Maucherat, A., Colin, C., & Llebaria, A. 2000, Experimental Study of External Occulters for the Large Angle and Spectrometric Coronagraph 2: LASCO-C2, Appl. Opt., 39, 3955

Breitling, F., Mann, G., Vocks, C., Steinmetz, M., & Strassmeier, K. G. 2015, The LOFAR Solar Imaging Pipeline and the LOFAR Solar Data Center, Astronomy and Computing, 13, 99

Cho, K., Chae, J., Lim, E.-K., Cho, K.-S., Bong, S.-C., & Yang, H. 2016, A New Method to Determine Temperature of CMES Using a Coronagraph Filter System, JKAS, 49, 45

Cram, L. E. 1976, Determination of the Temperature of the Solar Corona from the Spectrum of the Electron-Scattering Continuum, Sol. Phys., 48, 3

Cranmer, S. R. 2002, Coronal Holes and the High-Speed Solar Wind, Space Sci. Rev., 101, 229

Cranmer, S. R. 2009, Coronal Holes, Living Rev. Sol. Phys., 6, 3

Cranmer, S. R., & van Ballegooijen, A. A. 2005, On the Generation, Propagation, and Reflection of Alfven Waves from the Solar Photosphere to the Distant, ApJS, 156, 265

Cranmer, S. R., van Ballegooijen, A. A., & Edgar, R. J. 2007, Self-Consistent Coronal Heating and Solar Wind Acceleration from Anisotropic Magnetohydrodynamic Turbulence, ApJS, 171, 520

Fu, H., Li, B., Li, X., Huang, Z., Mou, C., Jiao, F., & Xia, L. 2015, Coronal Sources and In Situ Properties of the Solar Winds Sampled by ACE During 1999 – 2008, Sol. Phys., 290, 1399

Fujiki, K., Tokumaru, M., Iju, T., Hakamada, K., & Kojima, M. 2015, Relationship Between Solar-Wind Speed and Coronal Magnetic-Field Properties, Sol. Phys., 290, 2491

Goddard, C. R., Nisticò, G., Nakariakov, V. M., Zimovets, I. V., & White, S. M. 2016, Observation of Quasi-Periodic Solar Radio Bursts Associated with Propagating Fast-Mode Waves, A&A, 594, A96

Gong, Q., & Socker, D. 2004, Theoretical Study of the Occulted Solar Coronagraph, SPIE, 5526, 208

Grail, R. R., Coles, W. A., Klinglesmith, M. T., Breen, A. R., Williams, P. J. S., Markkanen, J., & Esser, R. 1996, Rapid Acceleration of the Polar Solar Wind, Nature, 379, 429

Gressl, C., Veronig, A. M., Temmer, M., Odstrcil, D., Linker, J. A., Mikic, Z., & Riley, P. 2014, Comparative

Study of MHD Modeling of the Background Solar Wind, Sol. Phys., 289, 1783

Hassler, D. M., Dammasch, I. E., Lemaire, P., Brekke, P., Curdt, W., Mason, H. E., Vial, J.-C., & Wilhelm, K. 1999, Solar Wind Outflow and the Chromospheric Magnetic Network, Science, 283, 810

Hayes, A. P., Vourlidas, A., & Howard, R. A. 2001, Deriving the Electron Density of the Solar Corona from the Inversion of Total Brightness Measurements, ApJ, 548, 1081

Howard, R. A., Sheeley, N. R. Jr., Michels, D. J., & Koomen, M. J. 1985, Coronal Mass Ejections – 1979–1981, J. Geophys. Res., 90, 8173

Illing, R. M. E., & Hundhausen, A. J. 1985, Observation of a Coronal Transient from 1.2 to 6 Solar Radii, J. Geophys. Res., 90, 275

Kohl, J. L., Noci, G., Antonucci, E., et al. 1998, UVCS/SOHO Empirical Determinations of Anisotropic Velocity Distributions in the Solar Corona, ApJ, 501, L127

Koutchmy, S. 1988, Space-Borne Coronagraphy, SSRv, 47, 95

Kurucz, R. L. 2005, New Atlases for Solar Flux, Irradiance, Central Intensity, and Limb Intensity, Memorie della Societa Astronomica Italiana Supplement, 8, 189

Kwon, R.-Y., Ofman, L., Olmedo, O., Kramar, M., Davila, J. M., Thompson, B. J., & Cho, K.-S. 2013, STEREO Observations of Fast Magnetosonic Waves in the Extended Solar Corona Associated with EIT/EUV Waves, A&A, 766, 55

Landini, F., Vivès, S., Romoli, M., et al. 2012, Optimization of the Occulter for the Solar Orbiter/METIS Coronagraph, SPIE, 8442, 844227

Landini, F., Romoli, M., Capobianco, G., et al. 2013, Improved Stray Light Suppression Performance for the Solar Orbiter/METIS Inverted External Occulter, SPIE, 8862, 886204

Lee, H., Moon, Y.-J., & Nakariakov, V. M. 2015, Radial and Azimuthal Oscillations of Halo Coronal Mass Ejections in the Sun, ApJL, 803, L7

Li, B., Xia, L. D., & Chen, Y. 2011, Solar Winds along Curved Magnetic Field Lines, A&A, 529, A148

Lionello, R., Linker, J. A., & Mikic, Z. 2001, Including the Transition Region in Models of the Large-Scale Solar Corona, ApJ, 546, 542

Liu, W., Title, A. M., Zhao, J., Ofman, L., Schrijver, C. J., Aschwanden, M. J., De Pontieu, B., & Tarbell, T. D. 2011, Direct Imaging of Quasi-Periodic Fast Propagating Waves of $\sim$2000 km s^{-1} in the Low Solar Corona by the Solar Dynamics Observatory Atmospheric Imaging Assembly, ApJL, 736, L13

Michalek, G., Shanmugaraju, A., Gopalswamy, N., Yashiro, S., & Akiyama, S. 2016, Statistical Analysis of Periodic Oscillations in LASCO Coronal Mass Ejection Speeds, Sol. Phys., 291, 3751

November, L. J., & Koutchmy, S. 1996, White-Light Coronal Dark Threads and Density Fine Structure, ApJ, 466, 512

Pinto, R. F., & Rouillard, A. P. 2017, A Multiple Flux-tube Solar Wind Model, ApJ, 838, 89

Plotnikov, I., Rouillard, A. P., Davies, J. A., et al. 2016, Long-Term Tracking of Corotating Density Structures Using Heliospheric Imaging, Sol. Phys., 291, 1853

Rougeot, R., Flamary, R., Galano, D., & Aime, C. 2017, Performance of the Hybrid Externally Occulted Lyot Solar Coronagraph. Application to ASPIICS, A&A, 599, A2

Nakariakov, V. M., Ofman, L., & Arber, T. D. 2000, Nonlinear Dissipative Spherical Alfvén Waves in Solar Coronal Holes, A&A, 353, 741

Ofman, L., Romoli, M., Poletto, G., Noci, G., & Kohl, J. L. 1997, Ultraviolet Coronagraph Spectrometer Observations of Density Fluctuations in the Solar Wind, ApJL, 491, L111

Parker, E. N. 1958, Dynamics of the Interplanetary Gas and Magnetic Fields, ApJ, 128, 664

Pascoe, D. J., Nakariakov, V. M., & Kupriyanova, E. G. 2013, Fast Magnetoacoustic Wave Trains in Magnetic Funnels of the Solar Corona, A&A, 560, A97

Purcell, J. D., & Koomen, M. J. 1962, Coronagraph with Improved Scattered-Light Properties, Report of NRL Progress (Washington, D.C.: U.S. GPO)

Reginald, N. 2001, MACS, an Instrument, and a Methodology for Simultaneous and Global Measurements of the Coronal Electron Temperature and the Solar Wind Velocity on the Solar Corona, PhD Thesis, University of Delaware, Source DAI-B 61/12, 6516

Richardson, J. D., & Kasper, J. C. 2008, Solar Cycle Variations of Solar Wind Dynamics and Structures, J. Atmos. Solar-Terrestrial Phys., 70, 219

Rotter, T., Veronig, A. M., Temmer, M., & Vrsnak, B. 2012, Relation Between Coronal Hole Areas on the Sun and the Solar Wind Parameters at 1 AU, Sol. Phys., 281, 793

Thernisien, A. F. R., Howard, R. A., & Vourlidas, A. 2006, Modeling of Flux Rope Coronal Mass Ejections, ApJ, 652, 763

Tokumaru, M., Kojima, M., & Fujiki, K. 2010, Solar Cycle Evolution of the Solar Wind Speed Distribution from 1985 to 2008, JGR, 115, A04102

van der Holst, B., Sokolov, I. V., Meng, X., Jin, M., Manchester, W. B. IV, Toth, G., & Gombosi, T. I. 2014, Alfvén Wave Solar Model (AWSoM): Coronal Heating, ApJ, 782, 81.

Wang, Y. M., Sheeley, N. R., Socker, D. G., Howard, R. A., & Rich, N. B. 2000, The Dynamical Nature of Coronal Streamers, J. Geophys. Res., 105, 25133

Wang, Y.-M., & Sheeley, N. R. Jr. 1990, Solar Wind Speed and Coronal Flux-Tube Expansion, ApJ, 355, 726

Yang, L. P., Feng, X. S., He, J. S., Zhang, L., & Zhang, M. 2016, A Self-Consistent Numerical Study of the Global Solar Wind Driven by the Unified Nonlinear Alfvén Wave, Sol. Phys., 291, 953

Yashiro, S., Gopalswamy, N., Michalek, G., St. Cyr, O. C., Plunkett, S. P., Rich, N. B., & Howard, R. A. 2004, A Catalog of White Light Coronal Mass Ejections Observed by the SOHO Spacecraft, J. Geophys. Res., 109, A07105